

Emitted Phonon Spectrum and Its Influence on the Detected Signal in Superconducting Sn Diodes

A. H. Dayem and J. J. Wiegand

Bell Telephone Laboratories, Holmdel, New Jersey 07733

(Received 20 December 1971)

We observed experimentally that the detected signal-vs-generator current deviates from linearity. The deviation has a shape similar to that of a Lorentzian. Preliminary arguments lead us to the conclusion that if the maximum deviation occurs at a generator voltage V_m , the emitted recombination peak should tend to a width given by $V_m - 2\Delta$. By calculating the spectrum of phonons emitted at a given generator voltage and hence the detector response signal, we have shown that the above prediction is essentially correct. We also give a brief discussion on the behavior of a superconductor when used as a phonon frequency convertor.

I. INTRODUCTION

In a previous paper¹ we presented experimental results pertaining to the behavior of a pair of superconducting Pb-Pb tunnel diodes when one diode is used as a phonon generator while the other is used as a detector. The diodes were evaporated on opposite faces of a sapphire single crystal which served as a medium for phonon transmission from generator to detector. Electron tunneling is used as a means for producing quasiparticle excitations in a fashion easily controlled by the applied voltage $V \geq 2\Delta$, where 2Δ is the superconductor's energy gap. Such excitations decay primarily via electron-phonon interaction and hence all input energy is transformed into phonon energy distributed in a band extending from zero energy to an intense peak at 2Δ followed by a rapidly decaying tail for higher energies. The phonons thus generated propagate in the sapphire crystal to the detector which is biased at a voltage $V_B < 2\Delta$. The detector response signal S is produced primarily by those phonons of energy $\omega \geq 2\Delta$ which, in breaking Cooper pairs, result in an increase in the steady-state quasiparticle population and hence an increase in the tunneling current. A great deal of information is contained in experimental plots of the signal S or its derivative as functions of V or I , the generator voltage and current, respectively. As previously shown¹ the basic character of such experimental curves can be deduced theoretically by the aid of a simple three-level system composed of two discrete quasiparticle levels at energies Δ and 3Δ , respectively, above the ground-state level, viz., the Fermi sea, which contains all Cooper pairs. With calculations based on this model we were able to show how the superconductor's density of states, by influencing the spectral distribution of the phonons emitted at a given voltage produces in the signal derivative the characteristic drop which immediately follows its sharp rise at $V = 4\Delta$. We were also able to show

the effect of the average recombination life time on the variation of S with I . Since the average recombination rate increases with increasing population, one finds that $S \propto I^{1/2}$ holds, if the phonon shower incident on the detector is sufficiently intense that the steady-state population it produces is large compared to the thermal population. In the opposite extreme, the so called linear limit, one obtains $S \propto I$.

Experimental evidence, however, points out that even in the linear limit there is an observable deviation from linearity in the dependence of S on I for $V < 4\Delta$. Such a deviation would arise from the factors not taken into account in the discrete three-level model, namely, the actual spectral distribution of the emitted phonons and the continuous spectrum of particle levels. In other words, this deviation from linearity should contain vital information about the spectrum of the generated phonons, and as we shall see later, it is possible to determine the width of the recombination phonons at $\omega \sim 2\Delta$ from the value of the generator voltage at which the maximum deviation occurs.

We begin this paper by outlining the experimental results which show the exact dependence of S and its derivative on I . The deviation from linearity as obtained experimentally is discussed, and a physical interpretation is given. In Sec. III, a theory is developed for calculating the emitted phonon spectrum at given generator voltage as well as the detector response signal. In both cases a simplified discrete-level model is used. The calculated phonon spectrum is discussed in detail in Sec. IV, while comparison between calculated and measured signals is carried out in Sec. V. Finally, in Sec. VI, some computed results are presented pertaining to the use of a superconductor as a phonon frequency convertor.²

II. EXPERIMENTAL RESULTS

The experimental techniques used here as well

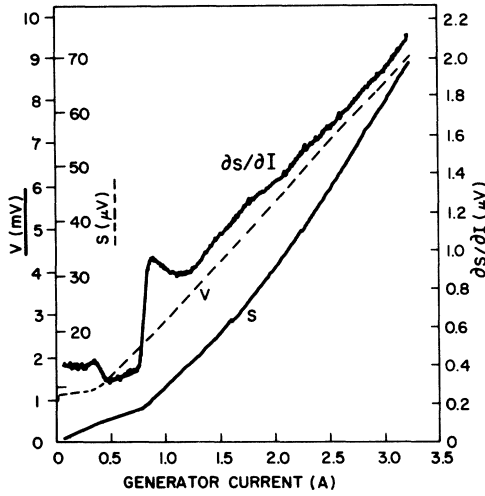


FIG. 1. Generator voltage V , detected signal S , and its derivative $\partial S/\partial I$ vs generator current I for samples No. 1.

as data acquisition and processing are exactly the same as those previously described.¹ Tin samples were prepared on two parallel faces of an intrinsic-germanium single crystal having dislocation density smaller than 1000 cm^{-2} .³ The barrier between the two stripes forming the diodes was prepared by oxidizing the first stripe in a stream of dry oxygen for 12–18 h. The resulting diode resistance is $\sim 0.005 \Omega$ for an area of 1 mm^2 . Good reproducibility was obtained with the resistance varying almost linearly with the oxidation time. Tin was used instead of lead because tin has a slower recombination rate and hence yields a signal-to-noise ratio one to two orders of magnitude larger than lead.

The experimental results are depicted in Figs. 1 and 2 for two different pairs of diodes. The generator resistance in Fig. 1 is ~ 3 times higher than that in Fig. 2. The sudden jumps (horizontal, vertical, or combination) in the curves labeled with S arise from zero-base-line instabilities of the sampling scope and have no physical significance. It is obvious that these instabilities produce no effects on the derivative measurements.

The salient features of the experimental results are summarized as follows:

(i) The signal S for $V < 4\Delta$ deviates markedly from its expected behavior. This deviation constitutes the major topic in this paper and will be discussed in greater detail.

(ii) At $V = 4\Delta$ there is a sharp kink in S which is reflected as a sharp rise in $\partial S/\partial I$. Here one encounters the onset of phonon generation with $\omega = 2\Delta$ coming from those quasiparticles injected at $E = 3\Delta$ which relax to the top of the gap.

(iii) The characteristic drop in $\partial S/\partial I$ for $4\Delta \leq V \leq 6\Delta$ shows clearly the effect of the superconduc-

tor's density of states on the spectral distribution of the emitted phonons.

(iv) For $V \geq 6\Delta$ the signal derivative rises monotonically but with undulating rate showing a point of steepest ascent at $V = 6\Delta$. However, subsequent onsets of a steep rise do not exactly coincide with the values $V = 2n\Delta$. This is to be expected because at these "quantum" points $V = 2n\Delta$ the maximum possible number of 2Δ phonons generated per particle is incremented by one for those excitations now injected at $E = (2n - 1)\Delta$.

We turn now to the main topic of this paper, namely, the dependence of S on I for $V < 4\Delta$ and its deviation from linearity. To derive the exact shape and magnitude of this deviation we do not use the measured values of S vs I . Instead, we use the measured values of $\partial S/\partial I$ in order to obtain greater numerical accuracy. In addition the results thus obtained are unaffected by the erratic behavior of the sampling-scope base line. The derivative in Fig. 2 is first numerically integrated using Simpson's rule in the range $0 \leq I \leq I(4\Delta)$. This gives the signal (in arbitrary units) as a function of the current as shown by the dashed line in Fig. 3. Note that it reproduces the corresponding portion of S in Fig. 2 with the erratic noise completely eliminated. The portion of the integrated signal for $I \leq 0.4 \text{ A}$ is fitted to a straight line using the least-squares fit to a Chebyshev expansion. The required deviation is then computed by subtracting from each value of the integrated signal the corresponding extrapolated value obtained from the straight-line fit. This yields the deviation from linearity depicted by the

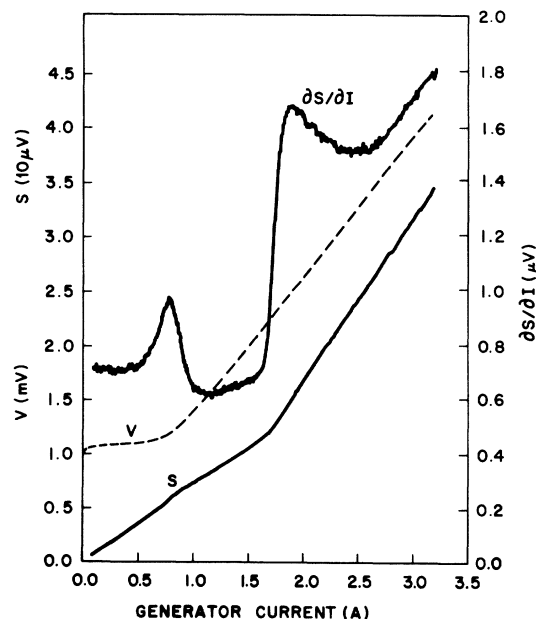


FIG. 2. V , S , and $\partial S/\partial I$ vs I for samples No. 2.

solid curve in Fig. 3. Except for the effect of the residual noise in that portion where the straight line fit was produced the deviation is everywhere positive, i. e., the signal is larger than the extrapolated linear dependence. We observe that the deviation has a Lorentzian shape with a maximum at $I = 0.95$ A and $V/\Delta = 2.45$. The maximum deviation is 7.93% of the value of the signal measured at the same voltage.

To interpret these results let us consider a group of particle levels in the energy range $\Delta \leq E \leq 1.2\Delta$. Single-particle transitions from one level to another within that group are associated with the emission or absorption of a phonon of energy $0 \leq \omega \leq 0.2\Delta$. Such transitions occur at a relatively slow rate because of two reasons. First, the phonon density of states is small and tends to zero as $\omega \rightarrow 0$. Second, the coherence factor entering the electron-phonon matrix element for such transitions goes to zero at the top of the gap. We shall refer to such a group of levels as "weakly coupled" because particles injected into any of these levels are hardly scattered to any other level within the group. For the sake of simplicity let us ignore recombinations in which the two participating particles originate from two different levels. With this in mind we may consider each level in a weakly coupled group as an independent source of recombination phonons. Let us now inject N particles in each of the two lowest-energy levels at Δ and E' . Two groups, each of approximately $\frac{1}{2}N$ phonons, will be emitted one of energy $\omega = 2\Delta$, the other of $\omega' = 2E'$. Since similar arguments hold for the detector, the two groups of phonons will produce two independent groups of quasi-

particle excitations in the detector, one at Δ and the other at E' . The steady-state populations are $N\tau$ at Δ and $N\tau'$ at E' where τ and τ' are the recombination life times at Δ and E' , respectively. The detected signal is proportional to $N(\tau + \tau') > 2N\tau$, since $\tau' > \tau$. Thus, if the incident shower contains phonons of energy $> 2\Delta$, the detected signal will have a positive deviation from linearity in its dependence on the generator current. Notice that the weakly coupled levels influence both the generation and the detection processes. Let us consider now what happens when we increase the injection width by increasing the generator voltage and current. As long as the particle levels which receive injection are weakly coupled, the deviation of the signal from linearity will increase, and the emitted phonon spectrum has a width at least as large as the injection width. When the injection width is made sufficiently large to include levels which are not weakly coupled, excitations injected into these latter levels will decay via a two-step process, namely, relaxation to a lower level followed by a recombination. It is obvious that at this point the deviation of the signal from linearity starts dropping. Since one may reasonably expect that the relaxation will transfer injected particles not only to the top of the gap but also to all weakly coupled levels adjacent to it, one may deduce that the emitted phonon spectrum at larger currents will settle to a width equal to $(V_m - 2)$, where V_m is the generator voltage, measured in units of Δ , at which the maximum signal deviation occurs.

The above discussion clearly shows that the dependence of the detected signal on the generator current and the deviation of this dependence from linearity contains sufficient experimental information which leads to the determination of the width of the recombination phonon peak in the emitted phonon spectrum. In the sample cited in Fig. 3 this width is equal to 0.45Δ . In Sec. III, a calculation of the emitted phonon spectrum followed by a computation of the signal it produces in the detector will verify these deductions.

III. THEORY

To calculate the emitted phonon spectrum and the response signal we use the following simplified model. This model consists of $K = 40$ discrete excited-particle levels in the range $\Delta \leq E < 3\Delta$, equally spaced in energy with a level separation $w = \frac{1}{20}\Delta$, in addition to the Fermi sea at zero energy which contains all Cooper pairs. Only electron-phonon interaction is taken into account. The phonons interacting with the particles fall into two groups: the relaxation phonons of energy nw with $1 \leq n \leq (K - 1)$ and the recombination phonons of energy $2 + (n - 1)w$ with $1 \leq n \leq K$. The limitation we impose on the energy ranges of excited particles and

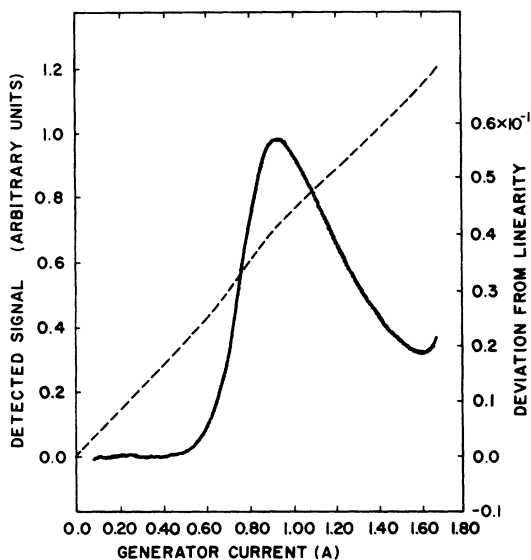


FIG. 3. Detected signal (dashed line), obtained by integrating $\partial S/\partial I$ in Fig. 2, and its deviation from linearity (solid line).

phonons simplifies the bookkeeping to a great extent. However, the theory as developed below can easily be extended to a wider energy range. The choice of the energy range in this paper is adequate for a comparison with the experimental results described in Sec. II.

We assume that the particles interact only with longitudinal phonons in normal processes. Under these assumptions the electron-phonon matrix element valid for the small energy range considered here can easily be obtained from Bardeen⁴ and Ziman.⁵ For a particle transition from state k to state k' with the absorption of a phonon of angular frequency ν the square of the matrix element is given by

$$|B_{kk'}|^2 = (\hbar/2MN\nu) (\frac{2}{3}E_F q)^2 g_q. \quad (1)$$

If the transition involves the emission of a phonon one has to replace the phonon occupation number g_q by $(1+g_q)$ to take into account both spontaneous and induced emissions. The phonon wave vector q satisfies the conservation of momentum $q = k - k'$. In (1), M is the atomic mass in g, N is the number of atoms/unit volume, V is the volume of the sample in cm^3 , and E_F is the Fermi energy in erg.

Next we need expressions which determine the transition probabilities in which a phonon of energy $\hbar\nu$ is emitted or absorbed in the superconducting state. These probabilities are given by expressions (4.25)–(4.27) of the Bardeen-Cooper-Schrieffer (BCS) paper.⁶ With proper modifications we shall adapt these expressions to the discrete level model described above. To outline the method we start with (4.25) of Ref. 6, viz., the expression

$$\left(\frac{2\pi}{\hbar}\right) \sum_{k, k' > k_F} 4 |B_{kk'}|^2 \left[1 - \left(\frac{\Delta^2}{EE'}\right)\right] f(1-f') \delta(E' - E - \hbar\nu), \quad (2)$$

which describes the rate of absorption of phonons of energy $\hbar\nu$ in particle transitions from states (k, E) to states (k', E') . Here the excited quasiparticles are taken to be in thermal equilibrium where the occupation number of a state E is given by the Fermi-Dirac distribution f . Note that the coherence factor that enters these transitions is of the form $(1 - \Delta^2/EE')$ and tends to zero if both E and E' tend to Δ .

In the discrete-level system we consider that each level contains all those excited particles which otherwise occupy states in the energy interval between this level and the next higher level. To convert the sum in (2) into a sum over events occurring between discrete levels, we integrate (2) over two small elements of phase space, one element between k and $k + dk$, the other between k' and $k' + dk'$. Keeping k constant, the integral over k' is carried out first using the spherical coordinates (q, θ, ϕ) with $\theta = \chi(k, q)$. The sum over k and k' is reduced

to a sum over k multiplied by the factor $2\pi(V/8\pi^3) \times q^2 dq \sin\theta d\theta$, where the integral over ϕ gives the factor 2π . Next we make the transformation $\theta \rightarrow E'$ using the relations

$$\epsilon' = (\hbar^2/2m)(k^2 + q^2 - 2kq \cos\theta) - E_F$$

and

$$E'^2 = \epsilon'^2 + \Delta^2,$$

where ϵ' is the Bloch energy of the state k' measured relative to Fermi energy E_F . The above factor is thus modified to

$$\frac{V}{4\pi^2} \frac{m}{\hbar^2} \frac{q}{k} \frac{E'}{\epsilon'} dq dE'.$$

Next we carry out the sum over k followed by the transformation $k \rightarrow E$ using the relations

$$\epsilon = \hbar^2 k^2/2m - E_F$$

and

$$E^2 = \epsilon^2 + \Delta^2,$$

which yield an additional multiplying factor of the form

$$\frac{V}{2\pi^2} \frac{m}{\hbar^2} k \frac{E}{\epsilon} dE.$$

Finally, one takes $\delta(E' - E - \hbar\nu) dE' = 1$ implying that E' must satisfy the conservation of energy $E' = E + \hbar\nu$. When these factors are inserted in (2) together with definition of the matrix element from (1) and the relations: $\nu = v_s q$, where v_s is the longitudinal sound velocity, $\omega = \hbar\nu$, $2mE_F = \hbar^2 k_F^2$, and $\omega_D^3 = 6\pi^2 N(\hbar v_s)^3$; the transition rate (2) can be put in the form

$$AA_{ij} f_i (1 - f_j) g_l, \quad (3)$$

with $j > i$ and $l = j - i$. The constant A and the matrix A_{ij} are given by

$$A = V k_F^4 \Delta^4 W^2 / 3\pi M v_s \omega_D^3 \quad (4)$$

and

$$A_{ij} = (1 - 1/E_i E_j) \rho_i \rho_j (E_j - E_i)^2. \quad (5)$$

Here we have used the normalized energies

$$W = w/\Delta = dE/\Delta,$$

$$E_i = E/\Delta = 1 + (i - 1)W,$$

$$E_j = E'/\Delta = 1 + (j - 1)W, \quad (6)$$

and

$$\omega_l = \omega/\Delta = E_j - E_i = lW.$$

The ratio of the density of states in the superconducting phase to that in the normal phase is

$$\rho_i = E_i / (E_i^2 - 1)^{1/2}. \quad (7)$$

The occupation probability of i th level is denoted by

f_i which in thermal equilibrium is given the Fermi-Dirac distribution, viz.,

$$f_i = (e^{\beta E_i} + 1)^{-1}. \quad (8)$$

In the present model f_i is the ratio of the number of particles occupying the i th level to the number of states belonging to that level. Similarly, g_i gives the ratio of the number of phonons of energy ω_i to the total number of phonon states belonging to the level ω_i . In thermal equilibrium g_i is given by the Bose-Einstein distribution

$$g_i = (e^{\beta \omega_i} - 1)^{-1}, \quad (9)$$

where $\beta = \Delta/k_B T$, k_B is the Boltzmann constant, and T is the temperature. Note that the phonon density of states is proportional to ω_i^2/ω_D^3 as in the Debye model where ω_i^2 is included in A_{ij} and ω_D^3 in A .

The transition rate in (3) gives the number of particles/sec which make a transition from level i to a higher level j absorbing an equal number of phonons of energy ω_i . It is evident from (3) and (5) that this rate is proportional to the number of particles in level i , the number of empty states in level j , and the number of phonons present of energy ω_i .

Other transitions rates are derived in a similar fashion. Thus for transitions from level i to a lower level j with the emission of phonon the rate is

$$AA_{ij}f_i(1-f_j)(1+g_l), \quad (10)$$

with $i > j$ and $l = i - j$. From (4.26) and (4.27) of Ref. 6 one obtains for transitions where a Cooper pair in the Fermi sea breaks with one particle going to level i , the other to j , and a phonon of energy $(E_i + E_j)$ is absorbed, the rate

$$AB_{ij}(1-f_i)(1-f_j)g'_i, \quad (11)$$

and for the inverse process the rate

$$AB_{ij}f_i f_j (1+g'_i), \quad (12)$$

where $l = i + j$ and g'_i is given by (9) after replacing ω_i by $\omega'_i = E_i + E_j$. The matrix B_{ij} is given by

$$B_{ij} = \frac{1}{2}(1 + 1/E_i E_j) \rho_i \rho_j (E_i + E_j)^2. \quad (13)$$

The manner in which the above rates is expressed is such that all constant terms are included in A while the coherence factors together with phonon and particle densities of state are included in the symmetric matrices A_{ij} and B_{ij} . The occupation numbers will constitute the variables in the detailed-balance equations. It is customary to write these equations in terms of the actual number of particles occupying a given level. It is obvious that with proper care one can use occupation numbers instead. We also assume that the above rates remain valid when the occupations numbers differ from their respective values in thermal equilibrium.

Thus, we will make the transformations $f_i \rightarrow N_i = f_i + n_i$, $g_i \rightarrow M_i = g_i + m_i$, and $g'_i \rightarrow M'_i = g'_i + m'_i$, where n_i , m_i , and m'_i are the excess population densities in the steady state of the excited system.

The detailed-balance equations are derived subject to the law of particle conservation which states that in the steady state the number of particles entering a given level per second equals the number leaving that level per second. We thus obtain sums over terms like

$$AA_{ij}[(1-N_j)N_i(1+M_i) - N_j(1-N_i)M_i], \quad (14)$$

which gives the net transition rate between a given level i and a lower level j . The first term in the square brackets is the number of particles per second leaving level i to level j emitting a phonon while the second term is the number per second that enters level i coming from j and absorbing a phonon. If one substitutes for the N 's and M 's in (14) their respective thermal-equilibrium values one finds that the term will vanish as required by the principle of detailed balance which states that in thermal equilibrium the number of particles per second which enter a given level by a particular path equals the number arriving per second by the reverse path. Note also that (14) can be immediately simplified to read

$$AA_{ij}[N_i(1+M_i - N_j) - N_j M_i], \quad (15)$$

where terms containing products of three occupation numbers have cancelled out. However, we still have products of two occupation numbers. To get a solution of the detailed-balance equations in closed form we have to linearize terms like (15) by assuming that the excess population in the steady state is small compared to thermal population. Thus, putting $N_i = f_i + n_i$ and $M_i = g_i + m_i$, with $n_i \ll f_i$ and $m_i \ll g_i$ in (15) the thermal equilibrium terms cancel as discussed above and we obtain to first order in n and m the expression

$$AA_{ij}[(1+g_i - f_i)n_i - (f_i + g_i)n_j - (f_j - f_i)m_i]. \quad (16)$$

The first-order detailed-balance equations thus obtained are as follows. For the i th particle level we get

$$\begin{aligned} & \sum_{j=1}^{i-1} A_{ij}[(1+g_i - f_j)n_i - (f_i + g_i)n_j - (f_j - f_i)m_i] \\ & + \sum_{j=i+1}^K A_{ij}[(g_i + f_j)n_i - (1+g_i - f_i)n_j + (f_i - f_j)m_i] \\ & + \sum_{j=1}^{K-i+1} B_{ij}[(g'_i + f_j)n_i + (g'_i + f_i)n_j \\ & \quad - (1 - f_i - f_j)m'_i] = Y_i, \quad (17) \end{aligned}$$

where the first sum is valid for $i > 1$ and $l = i - j$,

the second for $i < K$ and $l = j - i$, while the third for all i and $l = i + j$. The quantity Y_i is proportional to the number of particles per second injected by the tunneling current into the i th level, i. e.,

$$Y_i = 2I_i/eA, \quad (18)$$

where I_i is the tunneling current assigned to level i , e is the electronic charge, and the factor of 2 comes from the fact that identical excitations are produced by tunneling on either side of the barrier. The balance of the relaxation phonons m_i is given by

$$\sum_{n=1}^{K-l} A_{n,n+l} [(1+g_l - f_n)n_{n+l} - (g_l + f_{n+l})n_n] = \left(\sum_{n=1}^{K-l} A_{n,n+l} (f_n - f_{n+l}) + \gamma_l' \right) m_l, \quad (19)$$

which is valid for $1 \leq l \leq K-1$. The balance of the recombination phonons m_l' is given by

$$\sum_{n=1}^{l-1} B_{n,l-n} (g_l' + f_{l-n}) n_n = \left(\frac{1}{2} \sum_{n=1}^{l-1} B_{n,l-n} (1 - f_n - f_{l-n}) + \gamma_l' \right) m_l', \quad (20)$$

which is valid for $2 \leq l \leq K+1$. The coefficients γ_l and γ_l' are proportional to the rate at which the phonons escape from the film. They are also proportional to the phonon density of states as given by the Debye model. We thus have

$$\gamma_l = 9NV(\Delta/\omega_D)^3 W\gamma/A, \quad (21)$$

where the phonon escape rate γ is considered as a constant given by $\gamma = v_s/d$, where d is the combined thickness of both films.

In the numerical procedure one computes the coefficients of the individual n 's as given by the sums in (19) and (20) and thus transform these equations to the simpler form

$$\sum_{n=1}^K Q_{ln} n_n = U_l m_l, \quad (22)$$

with $1 \leq l \leq K-1$ and

$$\sum_{n=1}^{l-1} P_{l-1,n} n_n = V_{l-1} m_l', \quad (23)$$

with $2 \leq l \leq K+1$. Once the matrices Q and P and the vectors U and V are computed one can eliminate m_l and m_l' from the particle equation (17) using (22) and (23) to obtain

$$\sum_{j=1}^{i-1} A_{ij} \left((1+g_l - f_j)n_i - (g_l + f_i)n_j - U_i^{-1}(f_j - f_i) \sum_{n=1}^K Q_{ln} n_n \right) + \sum_{j=2+i}^K A_{ij} \left((g_l + f_j)n_i - (1+g_l - f_i)n_j \right)$$

$$+ U_i^{-1}(f_i - f_j) \sum_{n=1}^K Q_{ln} n_n + \sum_{j=1}^{K-i+1} B_{ij} \left((g_l' + f_j)n_i + (g_l' + f_i)n_j - V_{i-1}^{-1}(1 - f_i - f_j) \sum_{n=1}^{i-1} P_{i-1,n} n_n \right) = Y_i, \quad (24)$$

where the range for each sum is the same as that already defined for (17). After computing the coefficients, (24) reduces to

$$\sum_{j=1}^K R_{ij} n_j = Y_i \quad (25)$$

for $1 \leq i \leq K$ thus giving K linear equations to determine n_j , the excess population density in each of the K levels. Then using (22) and (23) together with n_n one obtains m_l and m_l' .

To evaluate the matrices A and B in (5) and (13) we need an appropriate definition of the density of states ρ_i which in turn determines the number of states to be assigned to the i th particle level. Because of the singularity at the gap of the theoretical density of states we encountered some difficulties. We finally decided on determining ρ_i in a manner consistent with the variation of the tunneling current with the voltage. This choice also enables us to determine two distinct densities of states one obtained from the theoretical variation of the tunneling current with the voltage using the BCS density of states, while the other is obtained from the experimental current-voltage characteristic. At an applied voltage $V_n = 2 + (n-1)w$ the tunneling current J_n is given by⁷

$$J_n = C \Delta \int_1^{V_n} \rho(E) \rho(V_n - E) dE = C \Delta [V_n E(\alpha_n) - (2/V_n) K(\alpha_n)], \quad (26)$$

where C is the dc diode conductance, $K(\alpha_n)$ and $E(\alpha_n)$ are complete elliptic integrals of the first and second kind, respectively, and $\alpha_n = [1 - (2/V_n)^2]^{1/2}$. For the discrete level system we convert the integral in (26) into a sum to obtain

$$J_n = C \Delta W \sum_{j=1}^n \rho_j \rho_{n-j+1}, \quad (27)$$

where ρ_j is the density of states belonging to the j th level. The solution of (27) gives

$$\rho_1 = (J_1/J_0)^{1/2}, \quad \rho_2 = J_2/(2\rho_1 J_0),$$

and

$$\rho_n = \left(\frac{J_n}{J_0} - \sum_{j=2}^{n-1} \rho_j \rho_{n-j+1} \right) / 2\rho_1, \quad (28)$$

where $J_0 = C \Delta W$. With J_m either calculated from (26) or obtained from the experimental I - V characteristic (28) gives the required densities of states for the BCS and experimental cases as shown by the

solid and dashed lines in Fig. 4, respectively. In the experimental case the starting value J_1 had to be chosen sufficiently close to the inflection point on the I - V characteristic in order to obtain a smooth solution of (28). For each density we shall compute the emitted phonon spectrum and the detector response and discuss the significant role played by the density of states.

To calculate the number of particles per second injected by the tunneling current into the i th level one writes

$$J_n = \sum_{j=1}^n I_j$$

and uses (27) to get

$$I_i = J_n \rho_i \rho_{n-i+1} \left(\sum_{j=1}^n \rho_j \rho_{n-j+1} \right)^{-1}. \quad (29)$$

To calculate the response of the detector to incident phonons of a given spectrum only slight modifications in the above equations are required. The balance of the relaxation phonons is now given by

$$\sum_{n=1}^K Q_{in} n_n + \frac{J_i}{A} = U_i m_i, \quad (30)$$

while that of the recombination phonons is

$$\sum_{n=1}^K P_{i-1,n} n_n + \frac{J'_i}{A} = V_{i-1} m'_i, \quad (31)$$

where J_i and J'_i are the numbers of incident phonons of energies ω_i and ω'_i , respectively. Using (30) and (31) to eliminate m_i and m'_i in (17) and taking all terms containing J_i and J'_i to the right-hand side, the particle equation for the detector assumes the form (25) with Y_i given by

$$Y_i = \sum_{j=1}^{i-1} \left(\frac{A_{ij}(f_j - f_i)J_j}{U_i} - \sum_{j=i+1}^K \frac{A_{ij}(f_i - f_j)J_j}{U_i} \right)$$

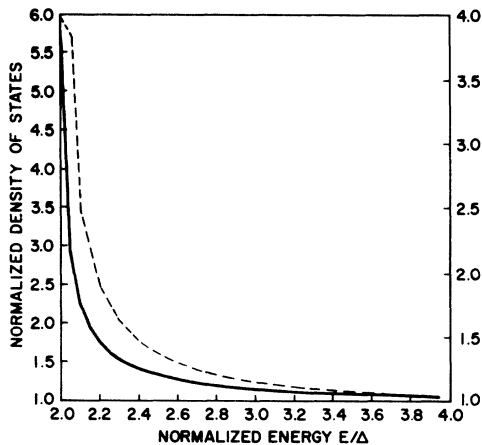


FIG. 4. Density of states assigned to the discrete levels; solid line for the BCS case (left scale), and dashed line for the experimental case (right scale).

$$+ \sum_{j=1}^{K-i+1} \frac{B_{ij}(1-f_i-f_j)J'_j}{V_{i-1}} \Bigg) / A, \quad (32)$$

where the first sum is valid for $2 \leq i \leq K$ and $l = i - j$, the second for $1 \leq i \leq K - 1$ and $l = j - i$, and the third for $1 \leq i \leq K$ and $l = i + j$.

Solution of (25) using (32) gives the steady-state excess population densities n_i in the K levels of the detector. Using the n_i thus obtained we calculate the detector signal using the expressions

$$S = D \sum_{i=1}^K n_i \rho_i \rho'_i, \quad (33)$$

where D is a constant, ρ_i is as defined by (28) while ρ'_i is given by

$$\rho'_i = [(E_{i+1} + V_B)^2 - 1]^{1/2} - [(E_i + V_B)^2 - 1]^{1/2}, \quad (34)$$

with V_B = detector bias in units of Δ .

We also use the solutions n_i together with (30) and (31) to compute m_i and m'_i , i. e., the spectral distribution of the phonons emitted by the detector. This distribution is certainly different from that of the incident phonons and reflects the effectiveness of the superconductor as an energy convertor.² It is obvious that Eqs. (30)–(32) can be used to calculate the output phonon spectrum resulting from an arbitrary input distribution of J_i and J'_i . Using a constant-input distribution we will compute the output distribution and the conversion efficiency.

In the numerical calculation one has to insure the validity of the results obtained by finding out whether they fulfil some conservation law. In calculations pertaining to phonon generation the total number of recombination phonons emitted should exactly equal one-half the number of injected particles. In the detector we use energy conservation as a check to insure that the total input energy in the incident phonons is exactly equal to the total output energy in the emitted phonons. All calculations were carried out in double precision and the conservation laws were fulfilled at least up to eight digits.

In Secs. IV–VII, we discuss the properties of the calculated spectrum and compare the computed detector response with that obtained experimentally. The calculations are carried out for a Sn–Sn diode of $d = 3000 \text{ \AA}$ and $V = 3 \times 10^{-7} \text{ cm}^3$. From the experimental I - V characteristic we took $\Delta = 0.57 \text{ meV}$ corresponding approximately to the onset of the steep rise in the current. The operating temperature is $\sim 1.05 \text{ }^\circ\text{K}$ giving $\beta = 6.3$. From McMillan,⁸ we obtained the density of states for one spin at the Fermi level $= N(0) = 0.883 \times 10^{22} \text{ eV}^{-1} \text{ cm}^{-3}$, $E_F = 10.33 \text{ eV}$, and $\omega_D = 0.01723 \text{ eV}$. Once the occupation numbers n_i and m_i are computed one obtains the number of particles in a given level $= 2N(0)V\Delta W\rho_i n_i$ and the number of phonons escaping into the substrate $= 9NV(\Delta/\omega_D)^2 \gamma W\omega_i^2 m_i$.

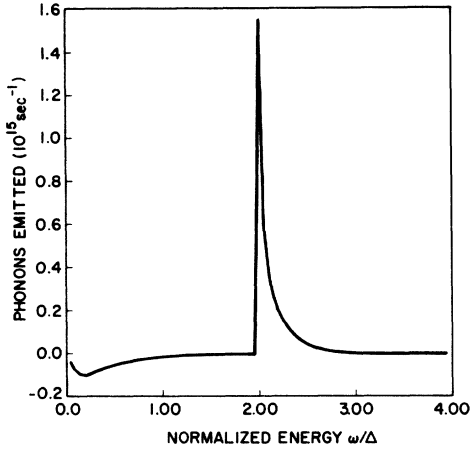


FIG. 5. Emitted phonon spectrum with injection into level 1 only ($N=1$).

IV. CALCULATED PHONON SPECTRUM

As pointed out previously the emitted spectra are calculated for two, distinct, particle densities of states, one representing the BCS case, the other the experimental case as depicted respectively by the solid and dashed curves in Fig. 4. In this section we will discuss the variation of the emitted spectrum with increasing injection width and point out the effects which may be attributed to coherence as well as those which are due to the density of states. For simplicity we will use the bracket (i, j) to denote either a transition from level i to level j with the emission (absorption) of a phonon for $i > (<)j$, or a recombination (pair breaking) involving a particle in level i and a particle in level j with the emission (absorption) of a phonon. In referring to the relaxation (recombination) phonons we will use the integer $l(l')$ to denote a phonon of normalized energy $\omega_l = lW[\omega_{l'} = 2 + (l' - 1)W]$, with $l = |i - j|$ ($l' = i + j - 1$). The injection width will be denoted by N , the number of levels receiving excited particles via tunneling at an applied voltage $V = 2 + (N - 1)W$.

When injection is limited to level 1 only, i. e., $N=1$ and $V=2$, the distribution in energy of the number of phonons emitted per second has a sharp peak at $\omega' = 2$ as depicted in Fig. 5. The width of this peak measured in units of Δ is 0.041 for the BCS case and 0.075 for the experimental case. Obviously this finite width is produced by transitions $(1, j)$ where a considerable fraction of the particles injected into level 1 are scattered by the thermal phonons to higher levels whence their subsequent recombination results in the emission of phonons of $\omega' > 2$. Indeed, one finds that only 0.42 of the total number of particles injected into level 1 recombine directly to the Fermi sea. Thus, if

y_1 denotes the number of phonons of $\omega = 2$ and y_t the total number of recombination phonons emitted per second, one finds $y_1/y_t = 0.42$.

It is obvious that for $N=1$ the transitions $(1, j)$ will result in a net absorption of phonons for all l as shown in Fig. 5 by the negative values for $\omega < 2$. This net absorption sustains an increase in the steady-state population of all levels $j > 1$ with a maximum at $j = 5$. The fact that the maximum absorption in Fig. 5 occurs at $l = 4$ rather than $l = 1$ shows clearly that adjacent levels are weakly coupled as discussed in Sec. II. Even when N is increased to 2 there is net absorption for all l indicating the extremely weak coupling between levels 1 and 2.

Let us see what happens when N is increased to 6. The emitted spectrum is shown in Fig. 6 and the particle occupation (i. e., the increase in the number of particles occupying a given level above its thermal value) is shown in Fig. 7. The width of the recombination phonons has increased to 0.28 which is larger than the injection width, $(N - 1)w = 0.25$. This is in agreement with the discussion in Sec. II where it was stated that as long as the levels which receive injection are weakly coupled the emitted spectrum has a width at least as large as the injection width. The idea that these levels may still be described as weakly coupled is elucidated by two observations obvious from Fig. 6. First the recombination spectrum has two peaks of approximately the same height (ratio ~ 0.74) at $l' = 1$ and $l' = 6$ corresponding to the equal peaks in the number of particles injected into levels 1 and 6, respectively. Second, there is still a large net absorption of low-energy phonons now extending over the range $6 \leq l \leq 10$.

Note that the second recombination peak occurs

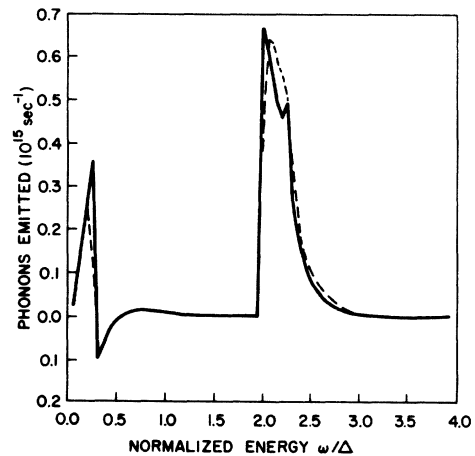


FIG. 6. Emitted phonon spectra with injection into 6 levels ($N=6$); solid line for BCS case and dashed line for the experimental case.

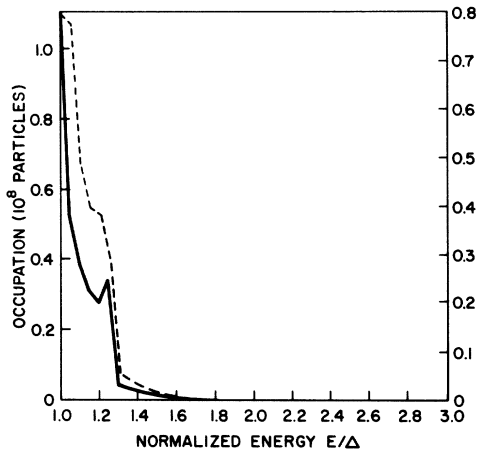


FIG. 7. Steady-state particle occupation for $N=6$; solid line for the BCS case (left scale), and dashed line for the experimental case (right scale).

at $l'=6$ and hence represents a recombination of the form (1, 6) rather than (6, 6) which would result from direct recombination of two particles from the highest level receiving injection ($N=6$) with the emission of a phonon $l'=11$. The reason for this is obvious, namely, the recombination (1, 6) has a faster rate than (6, 6) and since the particles participating in (1, 6) come from levels receiving maximum injection rate the second peak is almost as sharp as the first. For larger N the second peak always occurs at $l'=N$ and though it diminishes in magnitude and sharpness, it remains visible in a linear plot up to $N=31$.

The effect of the particle density of states is also quite clear. Because the BCS density of states has a sharp peak at the gap the excitations produced by tunneling will have two sharp peaks one at E_1 and the other at E_N . Thus the steady-state particle occupation and the emitted recombination spectrum will each have two sharp peaks at corresponding energies. Any deviations from the BCS density should be reflected in corresponding deviations in both the particle occupation and the spectrum. Hence going from the sharp BCS density to the rounded experimental density results in rounding and smearing of the peaks observable in the particle occupation and the phonon spectrum. These effects are clearly visible in Figs. 6 and 7. More important than the rounding, however, is the shift of the first peak of the recombination phonons from $l'=1$ for the BCS case to $l'=2$ in the experimental case. This shift will persist for larger N and will ultimately result in a larger width of the spectrum emitted in the experimental case.

In the low-energy portion of the spectrum shown in Fig. 6 one observes that there is net phonon

emission for $1 \leq l \leq N-1$, followed by net absorption for $N \leq l \leq 10$, and small broad-peaked emission for $11 \leq N \leq K$. Similar behavior is obtained for $N \leq 10$. However, with $N \geq 11$ there is net phonon emission for all l . This behavior is illustrated in Fig. 8 by the curves labeled z_N/I_N and z_{N-1}/I_N , where z_N is the number of relaxation phonons emitted per second in transitions like $(N+1, 1)$ and I_N is the number of particles per second injected into level N .

The energy at which the maximum number of relaxation phonons are emitted also varies with N . For $N \leq 14$ the maximum occurs at $l=N-1$. However, for $N > 14$ the maximum remains stationary at $l=13$. Then, it moves slowly with increasing N towards lower energy and finally settles at $l=10$ for $N \geq 31$. This behavior can be understood once the influence of the coherence factor on the electron-phonon interaction strength is clarified.

Once thermal equilibrium is disturbed by injecting excited particles into levels i , with $1 \leq i \leq N$, the rate of upward transitions induced by the thermal phonons to levels $j > N$ will increase. A new steady state is established with levels j now containing more particles than in thermal equilibrium. Whether these upward transitions will result in net phonon absorption over a certain energy range $l \approx j-1$ will depend on which of the levels $i \approx i_1$ make the major contribution to n_j . For example, if the levels i_1 are close neighbors to j the phonons absorbed have $l \approx 1$ and no net absorption is observed. If, however, the levels i_1 are remote from

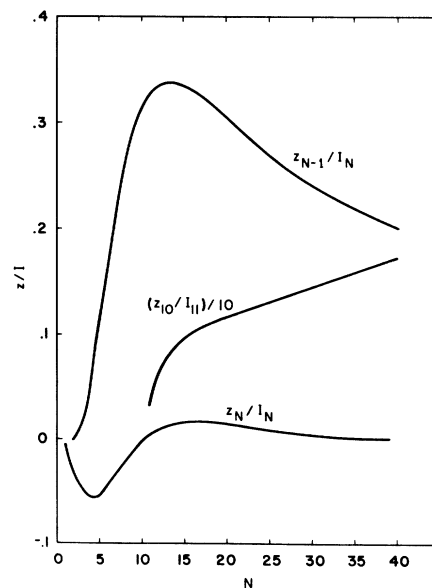


FIG. 8. Number of relaxation phonons emitted (z_l) relative to number of particles injected (I_l) and its variation with injection width N .

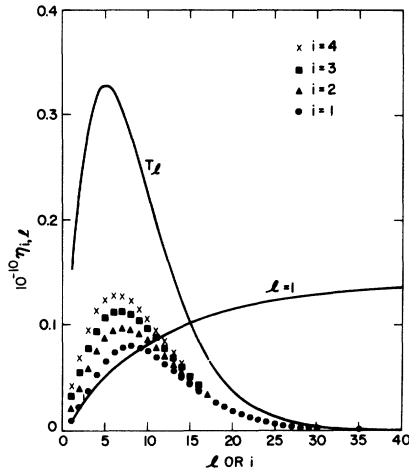


FIG. 9. Effect of coherence factor on induced emission and absorption of relaxation phonons. T_l is the thermal-phonon distribution and $\eta_{i,l} = T_l$ times coherence factor.

j net absorption of phonons for $l \approx j - 1$ is obtained. The rate of the transitions (i, j) with $i < j$ is dependent among other things on the number of thermal phonons T_l multiplied by the appropriate coherence factor. Denoting this product by $\eta_{i,l}$, where

$$\eta_{i,l} = T_l [1 - (E_i E_{i+l})^{-1}],$$

one observes that the coherence factor produces a large reduction in the interaction strength for small l and i . It also shifts the peak in T_l to larger values of l . This behavior is illustrated in Fig. 9 by four dotted curves representing $\eta_{i,l}$ vs l for fixed values of i . We also show in Fig. 9 $\eta_{i,1}$ vs i which represents the interaction strength to next neighbor ($l = 1$). We note that $\eta_{i,1}$ is smaller than $\eta_{i,i}$ up to $l \approx 10$. Beyond the region where the curves intersect $\eta_{i,1}$ gradually increases while $\eta_{i,i}$ drops rapidly to zero. Thus for $N < 10$ remote levels are sustaining the increased population in levels $j > N$ which results in the observed net phonon absorption. By referring to Fig. 9 one can easily interpret most of the properties described in the previous paragraphs as well as the behavior of the spectrum shown in Fig. 6 for $\omega < 2$.

Another important aspect is the effect of coherence on the rate of spontaneous emission of relaxation phonons ($\omega < 2$). Depicted in Fig. 10 is the phonon spectrum emitted with $N = K = 40$. Since g_l rapidly falls with increasing l (e. g., $g_1 = 2.7$, 0.12 for $l = 1, 6$, respectively), one expects that all particles injected into higher energy levels i (say $i > 15$) spontaneously relax to the immediate vicinity of level 1 (the top of the gap) emitting phonons with $l = i - 1$. Thus, the relaxation phonon spectrum should reflect the exact distribution of the injected

particles, i. e., it should start rising smoothly at $l \approx \frac{1}{2}N$ to a sharp peak at $l = N - 1$. Such behavior is completely absent in Fig. 10. In fact, if one plots z_{N-1}/I_N vs N , i. e., the number of phonons emitted in the relaxation $(N, 1)$ relative to the number of particles injected into levels N one finds, as shown in Fig. 8, that a maximum occurs at $N \approx 14$, where only one-third of the particles injected relax to level 1. The absence of the peak at $l = N - 1$ clearly indicates that particles injected in $i \approx N$ do not relax exclusively to the immediate vicinity of level 1 but rather spread over a large number of low-energy levels. This is further illustrated by the behavior of z_{10}/I_N with increasing N as depicted in Fig. 8. One finds that this ratio rapidly increases to unity at $N = 16$ and continues increasing beyond unity for larger N . A quantity proportional to the spontaneous emission rate is

$$\zeta_{i,j} = S_l [1 - E_i E_j]^{-1} \rho_j, \quad l = i - j$$

where S_l and ρ_j are the final phonon and particle states belonging to l and j , respectively. This quantity is plotted in Fig. 11 for various final states j as a function of the initial state i . One observes that all curves tend to come closer together for larger values of i . For example, relaxations from $i = 20$ to any level between 1 and 10 occur at various rates which lie within the same order of magnitude. Thus particles relaxing from level 20 are distributed among the lowest 10 levels while those relaxing from 30, for example, spread over 15 levels. This obviously results in a reduction in the fraction of particles going directly to level 1 and hence a reduction in z_{N-1}/I_N in Fig. 8. Another obvious consequence is the disappearance of the phonon peak expected at $l = N - 1$.

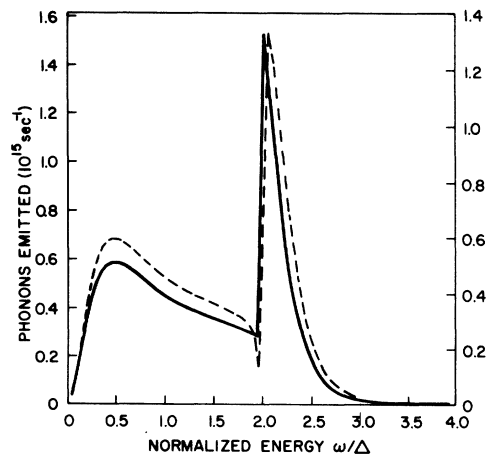


FIG. 10. Emitted phonon spectra with injection into all 40 levels; solid curve corresponds to the BCS case (left scale), dashed curve to the experimental case (right scale).

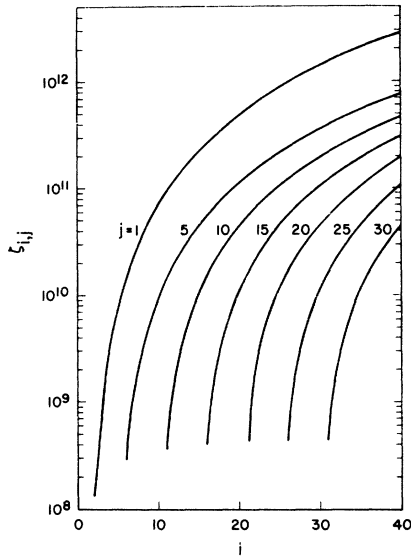


FIG. 11. Effect of coherence factor on spontaneous emission rate from initial level i to final level j .

If particles injected into high-energy levels relaxed exclusively to level 1, the peak in the recombination spectrum at $\omega \sim 2$ would continue to sharpen indefinitely with increasing N . The fact that relaxation distributes these particles over a large number of low-energy levels leads, therefore, to the conclusion that the recombination width will rapidly ($N \sim 15$) tend to a constant value. It also leads one to expect that even for $V > 4$ the spectral width will remain essentially the same as that calculated here for $V < 4$. The spectral widths calculated for the BCS and experimental cases tend

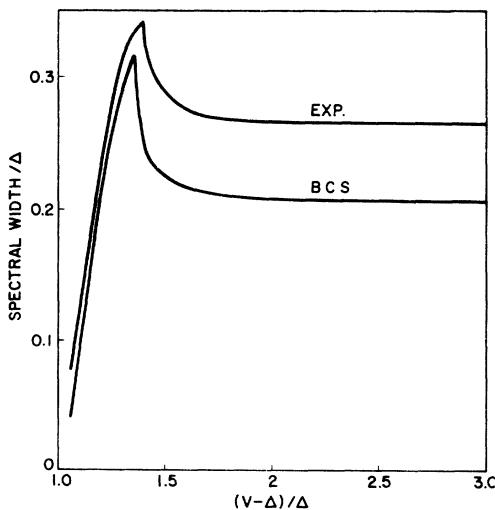


FIG. 12. Variation of the spectral width of the recombination peak with generator voltage.

to the values 0.206 and 0.265, respectively, as shown in Fig. 12. The odd shape of the curves at low voltage comes from the second recombination peak shown in Fig. 6. As mentioned previously, this peak occurs at $l' = N$. With increasing N the peak slides down the curve towards higher energy causing the width first to rise to an abnormally high value and then to drop rapidly and tend to its final value.

Of particular interest are the quantities $2y_1/I_1$ and y_1/y_t depicted in Fig. 13. They illustrate in the simplest manner the behavior of the system as previously described. The quantity $2y_1/I_1$ determines the number of particles recombining from level 1 relative to the number injected into that level. It hence determines the outcome of the two competing processes, namely, particle loss from level 1 to higher levels due to thermal-phonon absorption and particle gain in level 1 due to emission from higher levels. One finds that the loss prevails for $N < 12$ while the gain steadily rises with increasing $N > 12$. In spite of this steady rise in gain one finds that the ratio y_1/y_t tends to a constant for $N > 12$. This indicates that the spectral width will not continue to decrease with increasing $2y_1/I_1$ but will rather tend to a constant value as previously discussed. It is interesting to note that only ≈ 0.174 of the total number of recombination phonons emitted have an energy exactly equal to the gap.

V. COMPARISON BETWEEN CALCULATED AND MEASURED SIGNALS

As discussed in Sec. III, the phonon output from the generator at a given N is taken as input into

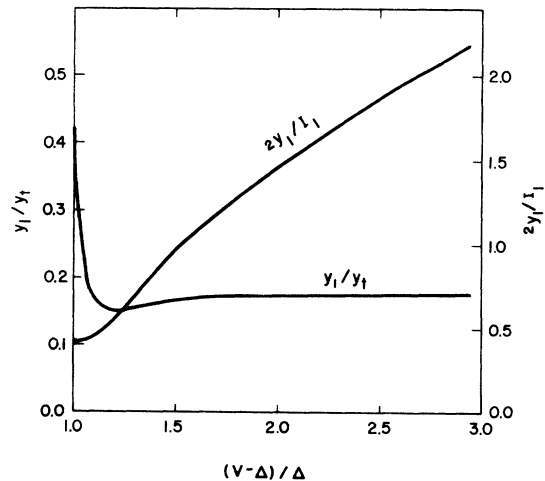


FIG. 13. Number of phonons y_1 emitted due to recombinations from level 1 relative to either the number of particles I_1 injected into level 1, or the total number of recombination phonons y_t .

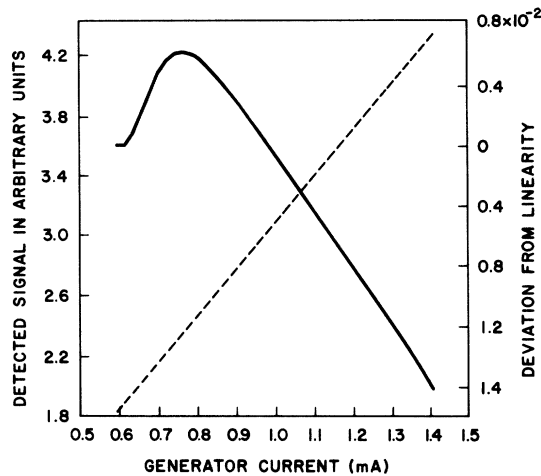


FIG. 14. Detected signal (dashed) and its deviation from linearity (solid) computer for the BCS case.

the detector. The response signal of the detector is then calculated at each value of N . Next, we determine a straight line passing through the first two points on the curve representing the signal as a function of the generator current. We assume that this straight line represents the linear response. The deviation is then calculated by subtracting values given by the straight line from the corresponding values of the computed signal.

The results computed for the BCS case are depicted in Fig. 14. These results agree in two respects with what we expected. First, the initial deviation is positive and rises to a maximum. Second, the magnitude of the deviation relative to the signal is small. At the position of the maximum, the ratio of the deviation to the signal is only 2.63×10^{-3} . The smallness of the deviation in the BCS case was expected because of the sharp peak in the density of states at the edge of the gap. It is obvious that this density of states, in influencing first the generation and then the detection processes, will result in a steady-state population in the detector which is quite sharply peaked at level 1. The contribution of level 1 to the signal current is, therefore, relatively large and hence a small deviation of the signal from the linear response is obtained.

The discrepancy, however, lies in the fact that the deviation in Fig. 14 goes negative at large N and that its maximum occurs at $V_m = 2.4$ instead of 2.2 as expected from the spectral width depicted in Fig. 12. We have no good explanation for this behavior. It is true that truncation errors may accumulate because of the large number of sums involved in the computation of the signal. This may happen in such a way as to produce systematic drift in the signal from its true value. Such er-

rors are apt to be more effective in the BCS case because of the small magnitude of the deviation relative to the signal. However, we have no estimate of the magnitude of such errors and the discrepancy should be attributed to an unknown cause.

The signal and its deviation computed for the experimental case are shown in Fig. 15. Comparison with Fig. 3 shows an excellent agreement between the computed and measured quantities. Both deviations, the computed and the measured, have almost identical shapes, remain always positive, and are of the same order of magnitude relative to their respective signals. At the position of the maximum the deviation amounts to 3.92% and 7.93% of the signal as determined from the computed and measured results, respectively.

In Fig. 15, the maximum deviation occurs at $V_m = 2.25$, while the computed spectral width is 0.265 as shown in Fig. 12. This is exactly the result we set out to prove, namely, that the width of the recombination peak is approximately given by $(V_m - 2)$. Since the experimental results in Figs. 2 and 3 give $V_m = 2.45$, we conclude that in the experiment the emitted recombination phonons have a width = 0.45. Obviously, we did not expect that the value of V_m measured experimentally will equal that obtained from the above calculation for two simple reasons. First, the transition rates in the experimental sample may be different than those adopted in the computation. Second, the steady-state populations of particles and phonons in the experiment may not be as small relative to the thermal populations as they should be to exert negligible change in the transition rates.

VI. SUPERCONDUCTOR AS FREQUENCY CONVERTER

Narayanamurti and Dynes² have shown experimentally that if a heat pulse is incident on a super-

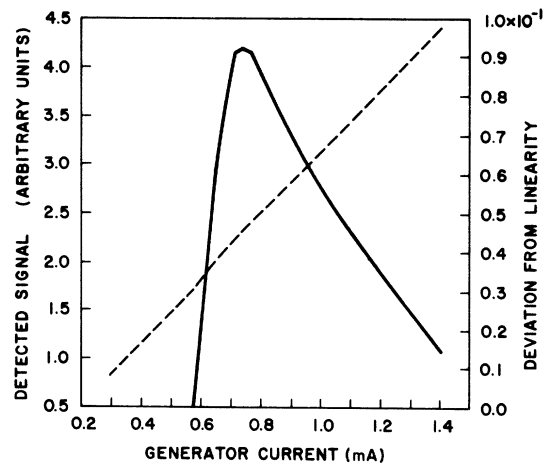


FIG. 15. Detected signal (dashed) and its deviation from linearity (solid) computed for the experimental case.

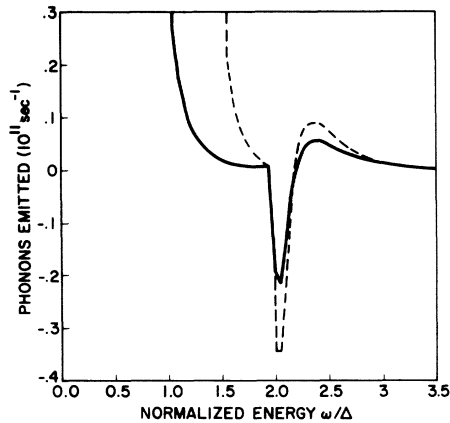


FIG. 16. Frequency "up" conversion from an input having a uniform distribution with cutoff at $\omega_c = 1$ (solid) and $\omega_c = 1.5$ (dashed).

conductor, the output pulse contains a sharp phonon peak at $\omega \sim 2$. Obviously, input phonons of energy $> 2\Delta$ will break Cooper pairs and the resulting quasiparticles relax and then recombine producing phonons of $\omega \sim 2$ in addition to low-energy phonons. To obtain an idea about the conversion efficiency of such a process we used part of the detector equations derived in Sec. III to calculate the spectral distribution of the phonon output corresponding to a given input. Two different input spectra were used, one as generated by a superconducting diode while the other has a uniform distribution (i. e., equal number of phonons in each level) with an arbitrary cutoff energy ω_c . The calculations were performed using the density of states belonging to the experimental case. We first consider an input having a uniform distribution with 0.5×10^{15} phonons in each level.

It is interesting to note that for $\omega_c < 2$ there is a small but finite phonon "up" conversion. The tail ends of the output distribution for $\omega_c = 1$ (solid) and $\omega_c = 1.5$ (dashed) are shown in Fig. 16. The behavior for $\omega \geq 2$ in Figure 16 is quite similar to that for $\omega \geq 0.3$ in Fig. 6. There is net phonon absorption for $\omega \approx 2$ followed by the "up" conversion (net emission) for $\omega > 2.2$. The incident phonons, being all of energy < 2 , can only excite the thermal quasiparticles present in upward transitions towards higher-energy levels. Since the thermal particles reside principally in the immediate vicinity of the gap edge, the partial depletion of their population due to incident-phonon absorption calls for Cooper pairs to break to establish the quasiparticle balance. This obviously results in net phonon absorption for $\omega \approx 2$. It is also obvious that the incident phonons have "over" populated particle levels of energy > 1.2 . The recombination from these levels gives the net phonon

emission for $\omega > 2.2$. In other words the incident low-energy phonons shift the center of mass of the quasiparticle distribution to higher energy resulting in the behavior depicted in Fig. 16. Since this process is critically dependent on the number of thermally excited particles, frequency up conversion is small and the output is roughly 4 orders of magnitude below the input.

The output spectrum shown in Fig. 17 was obtained from a uniform input distribution with $\omega_c = 4$. A good portion of the input high-energy phonons has been lost and their energy transferred to lower-energy phonons. The maximum gain occurs in a sharp output peak at $\omega \approx 2$. The output spectrum looks quite similar to that emitted from a superconducting diode (see Fig. 10) except that the horizontal axis in Fig. 17 is at 0.3×10^{15} .

The phonon conversion gain at a given energy, defined as the number of phonons gained (i. e., output-input) divided by the incident number is shown in Fig. 18. It is obvious that this curve is exactly valid only for a uniform input distribution with $\omega_c = 4$. Other input distributions with different cutoff will give a different conversion gain depending on the number of input phonons available for down conversion. One finds, for example, that when ω_c is increased from 2 the recombination peak starts from zero and rises almost proportionately to ω_c , to attain the value shown in Fig. 17 at $\omega_c = 4$. It is expected that this rise will continue at an even faster rate with increasing $\omega_c > 4$. Similar behavior is observed for the peak at $\omega = 0.5$. However, the conversion loss (gain < 0) in Fig. 18 for $\omega > 3$ approaches a constant value ≈ 0.26 independent of the energy. Therefore, it is plausible to assume, that with an arbitrary input, the spectral distribution of the output will have a shape similar to Fig. 18 superposed on the input distribution with the heights

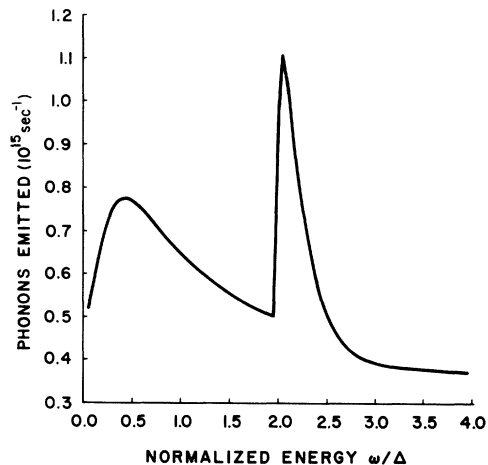


FIG. 17. Frequency "down" conversion from an input uniform distribution with $\omega_c = 4$.

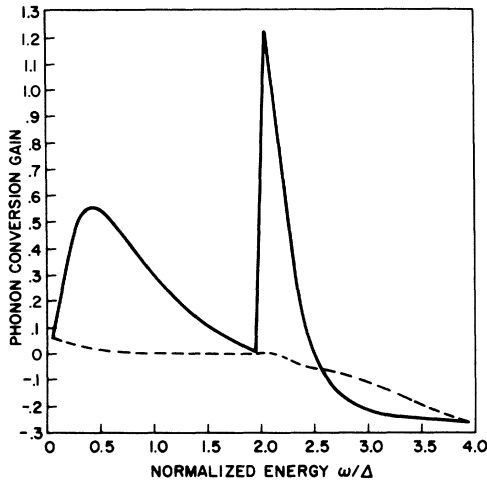


FIG. 18. Phonon conversion gain for two different input spectra: solid for a uniform distribution with $\omega_c=4$ and dashed for that generated by a superconducting diode shown in Fig. 10.

of the peaks at $\omega=0.5$ and 2 adjusted in accordance with the number of input phonons available for down conversion.

The dashed curve in Fig. 18 gives the conversion gain when the input has an identical distribution to that emitted by a superconductor for the case shown

in Fig. 10. We note that the conversion loss for high-energy phonons is of the same order of magnitude obtained for uniform distribution. However, since the input contains a small number of high-energy phonons available for down conversion, the conversion gain under the recombination and relaxation peaks is small. Thus, in this case the output spectrum looks almost identical to the input with only minor changes taking place.

VII. SUMMARY

We observed experimentally that the detected signal versus generator current deviates from linearity. The deviation has a shape similar to that of a Lorentzian. Preliminary arguments lead us to the conclusion that if the maximum deviation occurs at a generator voltage V_m , the emitted recombination peak should tend to a width given by $V_m - 2$. By calculating the spectrum of the phonons emitted at a given generator voltage and hence the detector signal response to such incident phonon distribution we have shown that our prediction was essentially correct.

At this point it seems worthwhile to extend the calculation of the spectrum to generator voltages $>4\Delta$ and to investigate the effect of different phonon escape rates γ , as well as the effect of umklapp processes on the emitted spectrum.

¹A. H. Dayem, B. I. Miller, and J. J. Wiegand, Phys. Rev. B **3**, 2949 (1971).

²V. Narayanamurti and R. C. Dynes, Phys. Rev. Letters **27**, 410 (1971).

³Phonon transmission through Ge single crystals with low dislocation density is at least as good as that in sapphire. Also, since the development of Syton polishing techniques, almost perfectly smooth surfaces with negligible scratches and digs can be obtained on Ge.

⁴J. Bardeen, Phys. Rev. **52**, 688 (1937).

⁵J. M. Ziman, *Electrons and Phonons* (Oxford U. P.,

London, England, 1960). The expressions used in deriving the matrix element in Eq. (1) can be found on pp. 182, 187, 200, and 161.

⁶J. Bardeen, L. N. Cooper, and J. R. Schrieffer, Phys. Rev. **108**, 1175 (1957).

⁷D. H. Douglas, Jr. and L. M. Falicov, in *Progress in Low Temperature Physics*, edited by C. J. Gorter (Wiley, New York, 1964).

⁸W. L. McMillan, Phys. Rev. **167**, 331 (1968). See Table III and Eq. (32).